J. Fluid Mech. (1984), *vol.* 141, *pp.* 365–390
Printed in Great Britain

Wave speeds in wavy Taylor-vortex flow

By GREGORY P. KING†, Y. LI, W. LEE, HARRY L. SWINNEY

Department of Physics, University of Texas, Austin TX 78712

AND PHILIP S. MARCUS‡

Department of Mathematics, Massachusetts Institute of Technology, Cambridge, MA 02139

(Received 8 June 1983 and in revised form 24 October 1983)

The speed of travelling azimuthal waves on Taylor vortices in a circular Couette system (with the inner cylinder rotating and the outer cylinder at rest) has been determined in laboratory experiments conducted as a function of Reynolds number R, radius ratio of the cylinders η, average axial wavelength $\bar{\lambda}$, number of waves m_1 and the aspect ratio Γ (the ratio of the fluid height to the gap between the cylinders). Wave speeds have also been determined numerically for axially periodic flows in infinite-length cylinders by solving the Navier–Stokes equation with a pseudospectral technique where each Taylor-vortex pair is represented with 32 axial modes, 32 azimuthal modes (in an azimuthal angle of $2\pi/m_1$) and 33 radial modes. Above the onset of wavy-vortex flow the wave speed for a given η decreases with increasing R until it reaches a plateau that persists for some range in R. In the radius-ratio range examined in our experiments we find that the wave speed in the plateau region increases monotonically from 0.14Ω at $\eta = 0.630$ to 0.45Ω at $\eta = 0.950$ (where the wave speed is expressed in terms of the rotation frequency Ω of the inner cylinder). There is a much weaker dependence of the wave speed on $\bar{\lambda}$, m_1 and Γ. For three sets of parameter values (R, $\bar{\lambda}$, η and m_1) the wave speeds have been measured, extrapolated to infinite aspect ratio, and compared with the numerically computed values. For each of these three cases the agreement is within 0.1 %.

1. Introduction

In 1965 Coles reported measurements of the frequency of rotation (wave speed) of the travelling azimuthal waves in wavy vortex flow in a concentric cylinder system with the inner cylinder rotating and the outer cylinder at rest. He found that, at large rotation rates Ω of the inner cylinder, the wave speed approached $\frac{1}{3}\Omega$. This asymptotic wave speed was found to be independent of the number of waves m_1 or the axial wavelength λ of the vortices. Feynman, Leighton & Sands (1974) discussed Coles' results and remarked, 'There's a challenge. A simple number like $\frac{1}{3}$, and no explanation'.

We have measured wave speeds for radius ratios η ranging from 0.63 to 0.95, and we find that at large Ω the wave speed has a strong monotonic dependence on η, increasing by a factor of three within the radius-ratio range studied. Thus the simple value of $\frac{1}{3}\Omega$ is an accidental consequence of Coles' choice of 0.875 for the radius ratio.

† Present address: Royal Signals and Radar Establishment, Great Malvern, WR14 3PS, England.
‡ Present address: Division of Applied Sciences, Aiken Hall, Harvard University, Cambridge, MA 02138.

The travelling azimuthal wave mode we have studied is usually called *wavy-vortex flow*; we will often call it the one-travelling-wave flow to distinguish it from the two-travelling-wave flow that occurs at larger Reynolds number. The onset of wavy-vortex flow occurs only 4% above the critical Reynolds number R_c for the Taylor instability in the narrow-gap limit (Davey, Di Prima & Stuart 1968), while for cylinders with a large gap the waves do not appear until well beyond the onset of Taylor-vortex flow—e.g. for $\eta = 0.63$ the waves appear at about $5R_c$ (Cole 1981). In wavy-vortex flow both the inflow and outflow vortex boundaries are wavy; in addition the waves on the inflow and outflow boundaries are shifted in azimuthal phase angle, as figure 1 illustrates; such a flow with m_1 waves has an m_1 fold rotational symmetry and a 'shift-and-reflect' symmetry about the midplane ($z = 0$) of a vortex pair (Marcus 1984*b*):

$$\left.\begin{aligned} V_r(r,\phi,z) &= V_r(r,\phi+\pi/m_1,-z),\\ V_\phi(r,\phi,z) &= V_\phi(r,\phi+\pi/m_1,-z),\\ V_z(r,\phi,z) &= -V_z(r,\phi+\pi/m_1,-z). \end{aligned}\right\} \tag{1}$$

In an experimental study of the onset of wavy-vortex flow in systems with radius ratios between 0.20 and 0.95, Cole (1981) found that the 'conventional wavy vortices' of the type described above occur for all $\eta \geqslant 0.38$, but in the range $0.38 \leqslant \eta \leqslant 0.63$ other types of wavy modes were also found. Some of these other types of wavy modes have been studied by Snyder (1970), Mullin & Benjamin (1980), Lorenzen, Pfister & Mullin (1983) and L'vov, Predtechensky & Chernykh (1981).† Furthermore, different types of wavy modes that occur at large R have been studied by Zhang & Swinney (1984) and in flows between independently rotating cylinders by Andereck, Dickman & Swinney (1983) and Andereck, Liu & Swinney (1984). The only wavy-vortex flows to be considered in this paper will be the conventional wavy vortices of the type shown in figure 1.

At Reynolds numbers well beyond the onset of wavy vortex flow a second set of travelling waves appears, at least for large η (Shaw *et al.* 1982). These two-travelling-wave flows have usually been called modulated wavy-vortex flows (Gorman, Swinney & Rand 1981; Gorman & Swinney 1982). The two wavetrains have different speeds, while the numbers of waves, m_1 and m_2, can be the same or different. Two-travelling-wave flows do not have the shift-and-reflect symmetry of (1).

We have investigated the dependence of wave speed on the control parameters (Reynolds number, radius ratio and aspect ratio) and on the spatial state of the flow (characterized by the axial wavelength and azimuthal wavenumbers). Most of our measurements and all of our calculations have been made for one-travelling-wave flows. The notation will be described in §2, and the experimental methods will be discussed in §3. The experimental results will be presented in §4. Numerical and analytic results are presented in §5, and are compared with the experimental results in §6. Our work is discussed and compared with other experiments and theory in §7. The conclusions are presented in §8.

2. Notation

The system is characterized by the following control parameters: the radius ratio $\eta = a/b$, where a and b are respectively the inner and outer radii of the annulus; the Reynolds number $R = a\Omega d/\nu$, where Ω is the angular frequency of the inner

† A photograph of one of these other wavy modes can be found in figure 8 of Burkhalter & Koschmieder (1973).

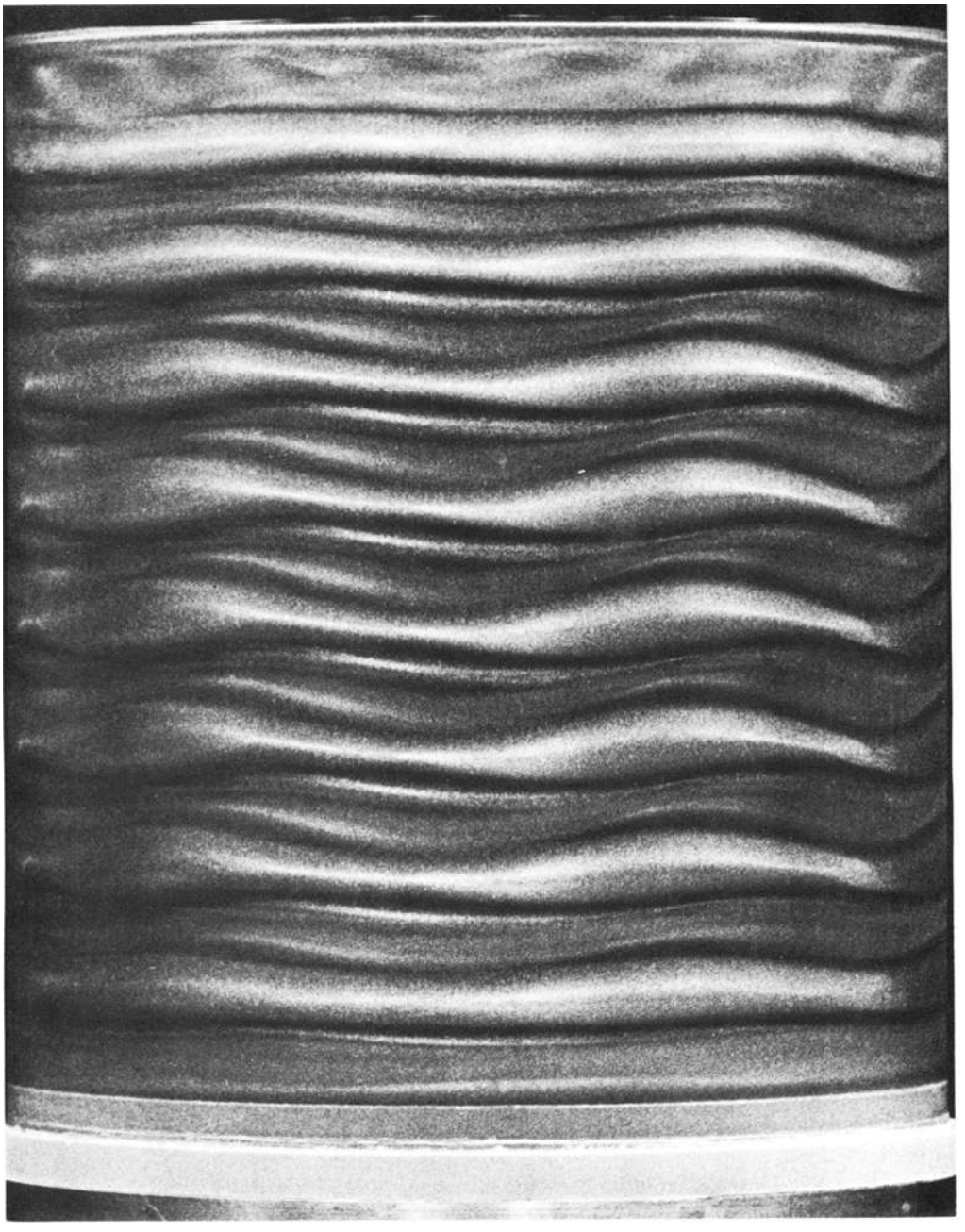

FIGURE 1. Photograph of the conventional wavy mode in wavy-vortex flow at $R/R_c = 7.1$, $\eta = 0.875$, $m_1 = 5$ and $\bar{\lambda}/d = 2.3$. Note that both the inflow and outflow boundaries are wavy, and that the waves at the inflow and outflow boundaries are shifted in azimuthal phase angle.

cylinder, ν is the kinematic viscosity and $d = b - a$; the aspect ratio $\Gamma = H/d$, where H is the height of the fluid. In this paper Reynolds numbers will be expressed relative to the critical Reynolds number R_c for the onset of Taylor-vortex flow in an infinite cylinder.

The speeds of the two travelling waves, s_1 and s_2, will be expressed in units of Ω.

η	a (cm)	$\Gamma_{\max}$	R_c†	Upper boundary
0.630	1.600	26	73.5	Rigid
0.730	1.854	36	82.9	Rigid
0.800	4.757‡	28	94.8	Free
0.840	2.134	38	105.2	Free
0.868	2.205	80	115.1	Free
0.877	2.228	80	119.1	Rigid
0.900	2.286	42	131.6	Free
0.950	5.649‡	115	185.1	Free

† Values for an infinite cylinder (from table 6.2 of DiPrima & Swinney 1981)
‡ Outer radius $b = 5.946$ cm; otherwise $b = 2.540$ cm

TABLE 1. Apparatus-parameter values

Thus $s_1 = \omega_1/m_1\Omega$ and $s_2 = \omega_2/m_2\Omega$, where ω_1 and ω_2 are the frequencies corresponding to the passage of waves past a point of observation in the laboratory.

The spatial state of a flow with travelling azimuthal waves is specified by, in addition to m_1 and m_2, the axial wavelength λ. In a cylinder of finite length, λ varies as a function of z, the variation becoming quite pronounced for states with $m_1 \leqslant 4$, particularly near certain stability boundaries (Ahlers, Cannell & Dominguez Lerma 1983; King & Swinney 1983; Park, Crawford & Donnelly 1983); in discussions of the experiments we will use the average axial wavelength defined by $\bar{\lambda} = 2H/N = (2\Gamma/N)\,d$, where N is the number of wavy Taylor vortices. Although λ is a function of z, the wave speeds are independent of z, that is, the travelling waves in each vortex pair are in phase (Fenstermacher, Swinney & Gollub 1979); see figure 1.

3. Experimental methods

3.1. *System parameters*

The parameters for our concentric-cylinder systems are given in table 1. The lower-fluid horizontal boundary was a Teflon ring attached to the outer cylinder; the upper boundary was left free in most of the experiments, but some measurements were made with a rigid upper boundary (another Teflon ring attached to the outer cylinder). All measurements for $\eta = 0.877$ were made with the cylinder system immersed in a water bath controlled in temperature to ± 0.02 K; measurements at other radius ratios were conducted at room temperature, which was usually constant to within 0.1 K during a measurement.

In the laser-Doppler velocimetry measurements nearly spherical titanium dioxide scattering particles with a diameter of 0.22 μm were suspended in a mixture of ethanol and methyl benzoate. (The concentrations of the fluids were adjusted so that the refractive index of the mixture exactly matched that of the glass outer cylinder at the laser wavelength, 0.488 nm. The kinematic viscosity of the mixture was measured to be 1.4 cS at 27.5 °C.) In these measurements the concentration of scattering particles was sufficiently dilute so that the scattering volume (about $30 \times 30 \times 100$ μm) almost never contained more than one particle. Therefore the average separation between particles was greater than 100 particle diameters. In the other measurements of the wave speed we used a mixture of commercially prepared Kalliroscope polymeric-flake solution diluted to 3% in water; this gives a 0.03% volume fraction of solid particles in the working fluid. The average separation

between the large flat Kalliroscope flakes ($25 \times 6 \times 0.07$ μm) was then of the order of the largest particle dimension.

Non-Newtonian effects such as shear thinning (that is, the dependence of the viscosity on the local shear rate) should be completely negligible in the laser-Doppler measurements, since the titanium dioxide particles are nearly spherical, non-deformable and widely separated. However, the close spacing of the Kalliroscope flakes requires us to show that the fluid remains Newtonian. We have varied the concentration of the Kalliroscope solution from 1.5 to 6% and have found from measurements of the inner-cylinder rotation rate at the onset of Taylor vortex flow that there is a Newtonian increase in the viscosity of 1.1% for each per cent increment in the concentration of Kalliroscope solution. The Reynolds numbers reported in this paper include this Newtonian correction.

For fixed Reynolds number and Kalliroscope concentrations in the range 1–3% we have found that within our experimental accuracy the wave speeds are independent of concentration; this independence of wave speed on particle separation distance indicates that there is no shear thinning.† This is not surprising since shear thinning is usually restricted to suspensions with very long and/or easily deformable polymers (Berman 1978). Another non-Newtonian effect that has been observed in laminar flow with suspended particles causes velocity fluctuations or 'early turbulence' (Zakin *et al.* 1977), which may be due to particle rotations (Jeffery 1923; Abernathy *et al.* 1980) – particles tumble as they are advected in a fluid with shear. If the tumbling perturbs the surrounding flow so that the perturbations influence the tumbling of very close neighbours, then the flow is non-Newtonian. The signature of this 'early turbulence' is the appearance in velocity power spectra of a broad band peak at a frequency of the order of the local strain rate. Since the strain rate is a strong function of position in Taylor–Couette flow, the broad peak is also a function of position. We have found no evidence of this broad peak in our power spectra. We note that in reported observations of 'early turbulence' (Zakin *et al.* 1977; Abernathy *et al.* 1980) the strain rates were of the order of 10^3 s^{-1}, while the maximum strain rate in the experiments reported here was of the order of 20 s^{-1}. Throughout the remainder of this paper we shall assume that the fluid is Newtonian and that the flow obeys the Navier–Stokes equation.

3.2. *Wave-speed measurements*

We have determined the speed of the azimuthal waves from laser-Doppler velocimetry measurements, scattered-light intensity spectra, stopwatch measurements and measurements in a rotating reference frame in which the waves were stationary.

The laser-Doppler technique was used on the system with $\eta = 0.877$ to measure the radial component of the fluid velocity at points in the middle of the gap between the cylinders. The velocity power spectra for one-travelling-wave flows have a single instrumentally sharp frequency component; in addition, there are sharp components at harmonics of the fundamental. Spectra for two-travelling-wave flows consist of two fundamental frequencies and their harmonics and combinations.

The other methods of measuring wave speeds were performed on flows that were visualized by the addition of Kalliroscope polymeric-flake solution to distilled water. A stopwatch was used to obtain the wave speeds for radius ratios $\eta = 0.630$, 0.730 and 0.800. For radius ratios $\eta = 0.840$, 0.868 and 0.900 the intensity of scattered laser light was detected by a photodiode and recorded in a computer as a function of time.

† A small but measurable non-Newtonian change in the wave speed was observed when the Kalliroscope concentration was increased to 8%, but this concentration is well beyond the 3% concentration used in the experiments reported in this paper.

It has been previously shown that the fundamental frequency components obtained from scattering intensity measurements are identical with those obtained from laser-Doppler measurements (Gorman, Reith & Swinney 1980).

Measurements in a rotating reference frame were made possible by mounting a television camera, focused on the flow, on a rotating table coaxial with the Couette system. The camera was connected through a slip ring to a video monitor in the laboratory frame. The table speed was adjusted until the wave pattern was motionless when viewed on the monitor. This method of measuring the wave speed was used for $\eta = 0.95$ because, at most Reynolds numbers studied at this radius ratio, there were defects in the flow pattern (even for $\Gamma = 20$), making interpretation of spectra difficult (defects or dislocations are discussed by Donnelly *et al.* 1980; Barcilon *et al.* 1979).

3.3. *State preparation*

The initial problem that must be resolved prior to an experimental investigation of wave speeds for different spatial states is how to produce on demand a state with particular values of N, m_1 and m_2 at some value of R, η, and Γ. This problem arises because the states that can be obtained in the circular Couette system are not uniquely determined by the control parameters – at a given η, R and Γ there are typically several different stable states N, m_1 and m_2 that can be obtained, depending on the flow history. Some of the different states can be produced simply by using different acceleration rates to go from rest to the final Reynolds number; however, only a small fraction of the accessible states of the system can be reached in this manner. This procedure must be supplemented by variations in either R or Γ (or both) to obtain the other possible states.

In our experiments we found that the most successful method of obtaining various states was the following. (1) The system was started suddenly from rest to a predetermined Reynolds number which previous experience had shown to result in the desired m_1. One try was usually sufficient but, if not, the system was repeatedly turned off and restarted until we were successful. (2) If N was less than what was wanted, fluid was allowed to flow in rapidly enough to increase N to the desired value. If N was too large, than the fluid was rapidly drained until the required number of vortices were obtained. (3) The aspect ratio was measured and fluid was either pumped in or out (slowly enough so that N would remain unchanged) until the desired $\bar{\lambda} = 2\Gamma/N$ was obtained. (4) When necessary, the Reynolds number was then slowly varied to the value at which the measurements were to be made.

The domains of stability for the various spatial states are sufficiently complicated that some variation in the order of application of the above steps was necessary in order to obtain some states. In general, however, we found that when the above procedure was supplemented with experience in the operation of a system with a particular radius ratio, there was little difficulty in obtaining any stable state in the one-travelling-wave flow regime for that radius ratio. The production of different states was easiest for radius ratios near 0.868, since for this radius ratio King & Swinney (1983) studied the stability of different one-travelling-wave states over a large range of Reynolds numbers and axial wavelengths.

4. Experimental results

We have found that the wave speed is a much more complicated function of the control parameters R, η and Γ, and the spatial state characterized by $\bar{\lambda}$, m_1 and m_2

than previously realized. This suggests that wave speeds will be a sensitive test of theory and of numerical simulations of wavy-vortex flows.

We now present the experimental results for the dependence of wave speed on Γ, $\bar{\lambda}$, m_1, m_2, R and η, in that order.

4.1. *Dependence of s_1 on aspect ratio*

The major difficulty in comparing numerical and experimental results is that experiments must necessarily be performed with cylinders of finite length and real end boundaries, while simulations nearly always assume infinitely long cylinders ($\Gamma = \infty$) (i.e. periodic boundary conditions in the axial direction). It is often claimed that finite-length effects should be negligible if the experiments are done in long cylinders; however, the length of 'sufficiently long cylinders' can vary greatly, depending on the property of interest and on R, η, m_1, m_2 and $\bar{\lambda}$. For example, Cole (1976) found that, with $\eta = 0.894$ and $\Gamma = 20$, the measured and calculated values for the onset of Taylor vortex flow differed by only 1%, while, in contrast, the measured Reynolds number for the onset of wavy-vortex flow was 15% higher than that predicted.

We have investigated the dependence of the wave speed on aspect ratio for only four cases. Such an investigation was not attempted for every case reported here for two reasons: (1) the time for the properties of a flow state to relax to their final values is already quite long for $\Gamma = 32$ and simply becomes prohibitively long for detailed studies at much larger Γ; (2) at large values of Γ there is an increased occurrence of defects and distorted flow patterns so that $\bar{\lambda}$, m_1 and m_2 are no longer well defined (King & Swinney 1983).

Measurements of the variation of wave speed with aspect ratio are shown for two cases in figure 2. The measurements of figure 2(*a*) were not taken beyond $\Gamma = 80$ because the experimental apparatus was not long enough, and the measurements of figure 2(*b*) extend only to $\Gamma = 45$ because, when Γ was increased further, there was a transition from $m_1 = 4$ to $m_1 = 3$ (that is, the domain of stability depends on aspect ratio; see King & Swinney 1983).

The data suggest that the Γ-dependence of s_1 can be described by functions that depend on $1/\Gamma$, for example,

$$s_1^{\alpha}(\Gamma) = s_1^{\alpha}(\infty) + \frac{\alpha}{\Gamma}, \tag{2}$$

$$s_1^{\beta}(\Gamma) = s_1^{\beta}(\infty) + \frac{\beta}{\Gamma}\exp\left(\frac{-\Gamma}{l}\right). \tag{3}$$

The results of least-squares fits of data to s_1^{α} and s_1^{β} are given in table 2. Both equations fit the data for all cases with an r.m.s deviation of only 0.01–0.03%, but there are systematic deviations which are in the opposite directions for the two equations; see the deviation plots in figure 2.

We have investigated the difference in wave speeds when the upper boundary was either a free surface or rigid (another Teflon ring attached to the outer cylinder) for a few cases and found a very weak effect, only on the order of 0.1% or less with $\Gamma = 32$ and $R/R_c \geqslant 4$; the effect should be even smaller at larger Γ.

4.2. *Dependence of s_2 on aspect ratio*

The speed of the second travelling wave was investigated only for $\eta = 0.868$, where the onset of the second wave is in the range $7 < R/R_c < 12$, depending on $\bar{\lambda}$, m_1 and

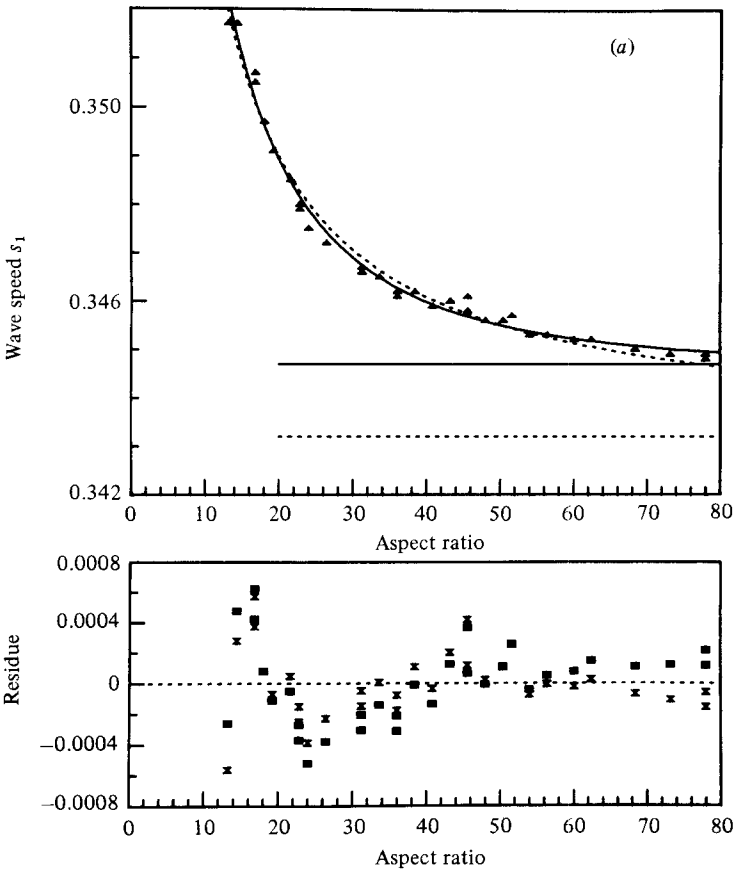

FIGURE 2(*a*). For caption see facing page.

Γ. The dependence of s_2 on Γ was found to be very weak, too weak to determine any functional dependence from the data, as figure 3 illustrates.

Although the aspect ratio dependence of the onset of two-travelling-wave flows was not investigated, we note from our measurements at $R/R_c = 10.95$ that such a dependence does indeed exist: whenever Γ was reduced below $\Gamma = 18$, the second travelling wave always disappeared.

4.3. *Dependence of s_1 on axial wavelength*

Figure 4 shows the wave-speed dependence on axial wavelength for a six-wave state in a sytem with $\eta = 0.868$ at $R/R_c = 3.98$ and $R/R_c = 5.97$. This figure and measurements for other states show that the functional dependence of s_1 on $\bar{\lambda}$ varies considerably, but that the total variation with $\bar{\lambda}$ is in general only a few percent for a given η, R, Γ, m_1 and m_2.

4.4. *Dependence of s_1 on the number of waves (m_1 and m_2)*

The data shown in figures 5(*a*, *b*) illustrate the dependence of s_1 on the number of azimuthal waves in a system with $\eta = 0.877$. Figure 5(*a*) compares s_1 for states that differ only in m_1 and figure 5(*b*) compares s_1 for states that differ only in m_2.

In figure 5 the change in s_1 for $\Delta m_1 = 1$ is only about 1.5%, and the change in s_1

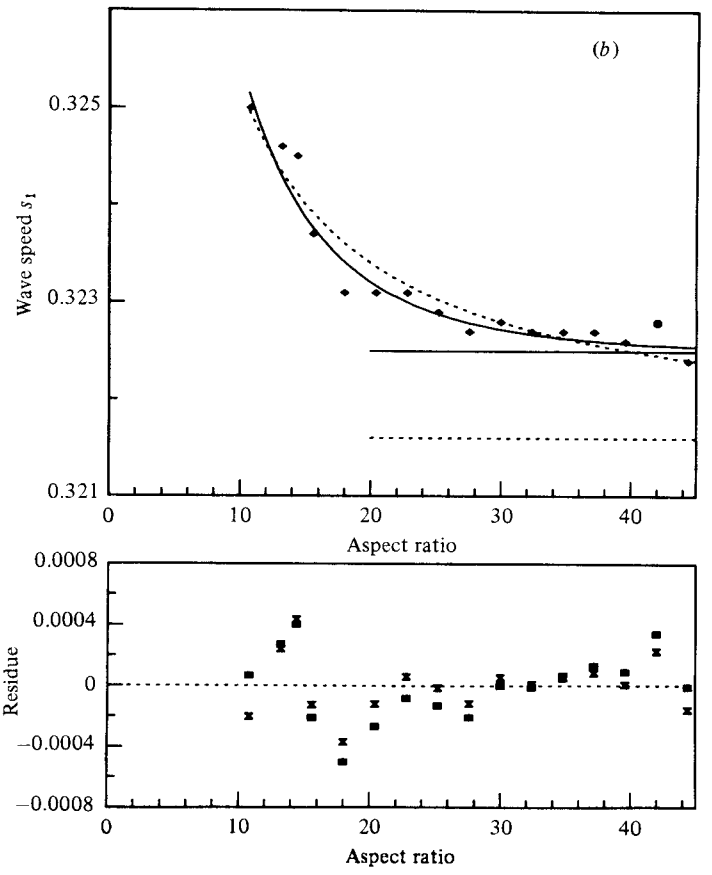

FIGURE 2. The dependence of wave speed s_1 on aspect ratio for $\bar{\lambda}/d = 2.4$, in a system with $\eta = 0.868$: (*a*) one-travelling-wave flow at $R/R_c = 3.98$, $m_1 = 6$; (*b*) two-travelling-wave flow at $R/R_c = 10.95$, $m_1 = 4$ and $m_2 = 4$. The dashed and solid curves are respectively least-squares fits to (2) and (3), and the horizontal dashed and solid lines are the corresponding values of the wave speed extrapolated to $\Gamma = \infty$. The lower graphs show the deviations of the data from (2), shown by the points ■, and from (3), shown by the points ⧗.

for $\Delta m_2 = 1$ is only 0.3% or less. For other states a similar weak dependence of s_1 and s_2 on m_1 and m_2 was observed.

Note in figure 5(*a*) that s_1 is larger for the state with the larger value of m_1. This relationship is not generally true. For example, for $R \leqslant 2R_c$ we found that s_1 decreased when m_1 was increased (also see Ahlers *et al.* 1983).

4.5. *Dependence of s_1 on Reynolds number*

Beyond the onset of wavy vortex flow the wave speed s_1 decreases monotonically with increasing R until it reaches a plateau, which extends over a wide range in R; then there is a small gradual increase in s_1 before the waves disappear. This dependence of s_1 on R is illustrated in figure 6 with data for a system with $\eta = 0.840$; the same kind of Reynolds-number dependence was observed at all radius ratios studied.

The Reynolds number at which the plateau begins and ends depends on m_1, m_2, and in particular on $\bar{\lambda}$. For example, as figure 4 illustrates with data at $R/R_c = 3.98$ and 5.97 for a state with $m_1 = 6$, s_1 decreases with R for $\bar{\lambda}/d < 2.54$ and increases for $\bar{\lambda}/d > 2.54$.

Fit to (2)

R/R_c	$\bar{\lambda}/d$	m_1	m_2	n†	$s_1^{\alpha}(\infty)$	α	r.m.s. deviation %
3.98	2.4	6	—	32	0.3432	0.116	0.026
3.98	3.0	6	—	23	0.3340	0.106	0.021
5.97	2.2	6	—	19	0.3368	0.025	0.014
10.95	2.4	4	4	16	0.3216	0.036	0.023

Fit to (3)

R/R_c	$\bar{\lambda}/d$	m_1	m_2	n†	$s_1^{\beta}(\infty)$	β	l	r.m.s. deviation %
3.98	2.4	6	—	32	0.3447	0.138	40.4	0.022
3.98	3.0	6	—	23	0.3354	0.171	28.2	0.013
5.97	2.2	6	—	19	0.3372	0.122	11.3	0.009
10.95	2.4	4	4	16	0.3225	0.063	13.9	0.019

† Number of data points

TABLE 2. Aspect-ratio dependence of the wave speed

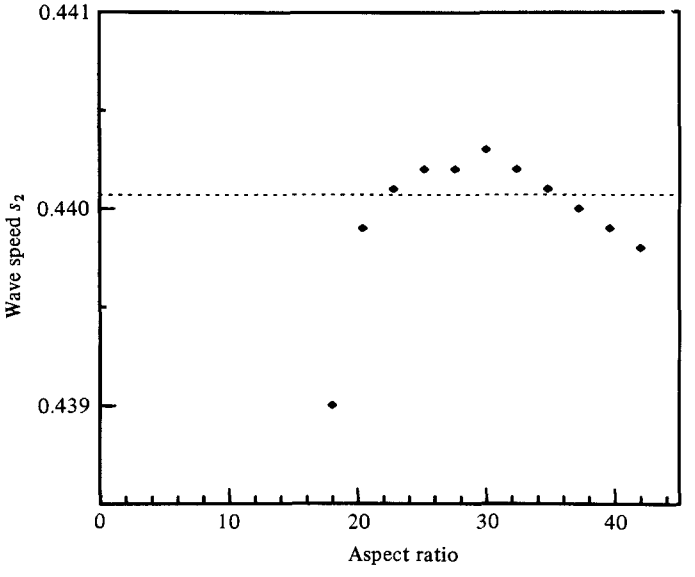

FIGURE 3. The dependence of the wave speed s_2 on aspect ratio for $\bar{\lambda}/d = 2.4$, in a system with $\eta = 0.868$, $R/R_c = 10.95$, $m_1 = 4$ and $m_2 = 4$. When Γ was reduced below 18 there was a transition to a one-travelling-wave flow.

At all radius ratios studied, the dependence of s_1 on m_1, m_2, $\bar{\lambda}$ and Γ in the plateau region was found to be small, at most a few percent.

4.6. *Dependence of s_1 on radius ratio*

In marked contrast with the weak dependence on m_1, m_2, $\bar{\lambda}$ and Γ, the wave speed was found to depend very strongly on radius ratio, as figure 7 illustrates. Note that the data at each radius ratio exhibit the general dependence on R described in §4.5.

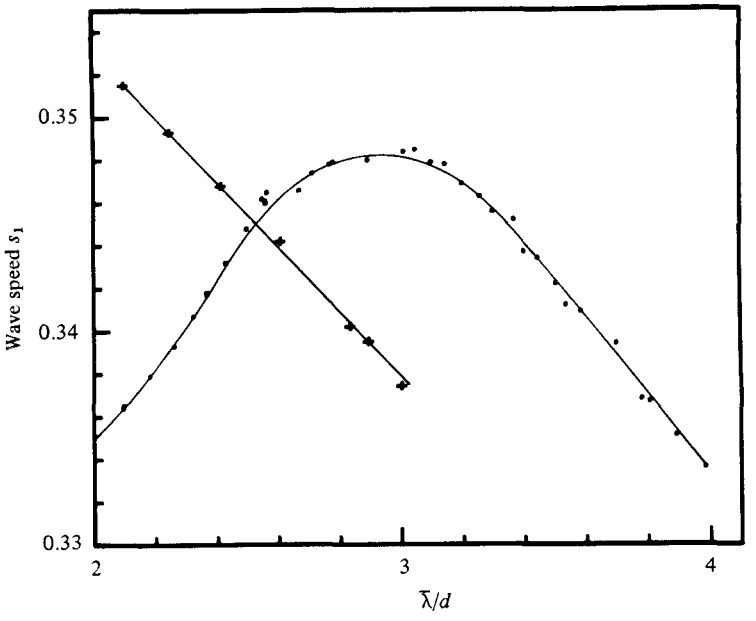

FIGURE 4. The dependence of wave speed s_1 on the average axial wavelength $\lambda/d = 2\Gamma/N$ in a system with $\eta = 0.868$ for two different Reynolds numbers (with $m_1 = 6$): $R/R_c = 3.98$ (+) and $R/R_c = 5.97$ (•). The number of vortices and the aspect ratio were varied simultaneously to keep $\Gamma \approx 33$ for the different values of $\bar{\lambda}$. The curves are drawn to guide the eye.

The Reynolds number $R/R_c \approx 11$ is in the plateau region for the wave-speed data at $\bar{\lambda}/d = 2.4$ for all radius ratios, as can be seen in figure 7; therefore we have chosen this Reynolds number for a comparison of wave speeds for different radius ratios. This dependence on radius ratio is shown in figure 8. The curve drawn through the points is a best fit to Chebyshev polynomials, as will be discussed in §6.

Summarizing the data, we find that to a good approximation the wave speed at large Reynolds number depends only on radius ratio.

5. Numerical and analytic studies

5.1. *Calculation of the wave speeds by numerical simulation*

Using an initial-value code with 33 radial Chebyshev modes, 32 Fourier azimuthal modes and 32 Fourier axial modes, we have numerically simulated several one-travelling-wave flows and determined the wave speeds. We assume *a priori* that the flow is axially periodic, and we simulate only one of the infinite array of vortex pairs. The calculations were performed with the primitive variables (the velocity components V_r, V_z, V_ϕ, and the pressure) rather than using a stream-function–vorticity representation. We used a pseudospectral method in which the multiplications were done by tabulating the primitive variables (which are real quantities) on a $33 \times 32 \times 32$ mesh of grid points in physical space, and the derivatives were computed in spectral space. In spectral space the velocity is represented by a set of $33 \times 32 \times 16$ complex spectral coefficients $\boldsymbol{a}_{n,m,k}(t)$:

$$V(r,\phi,z,t) = \sum_{n=0}^{33} \sum_{m=-15}^{16} \sum_{k=0}^{15} \boldsymbol{a}_{n,m,k}(t)\, T_n(r)\, \mathrm{e}^{\mathrm{i}m\phi} \mathrm{e}^{\mathrm{i}2\pi kz/\lambda} + \text{c.c.}, \tag{4}$$

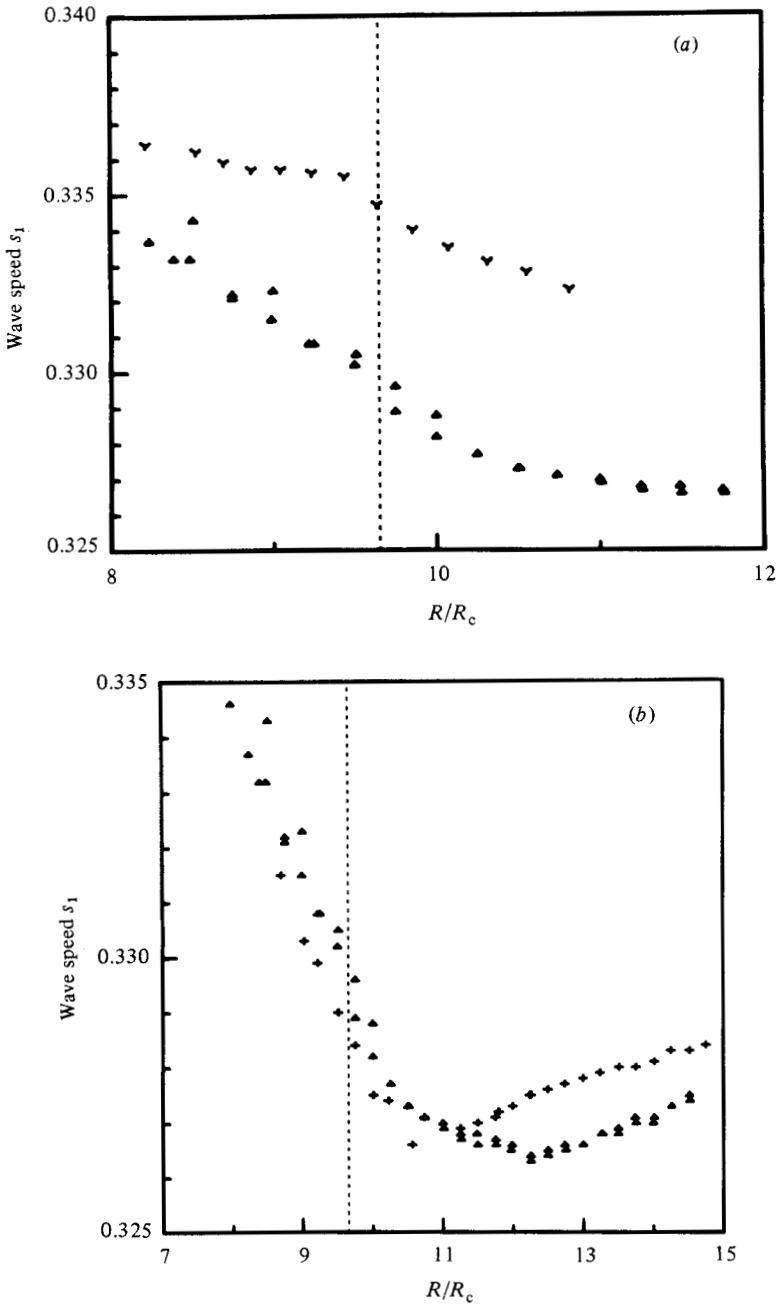

FIGURE 5. A comparison of wave speeds s_1 in flows with $\bar{\lambda}/d = 2.5$ and $\Gamma = 20$: (*a*) two flows with the same m_2 valves and different m_1 values ($m_1 = 4$, $m_2 = 4$ (▲); $m_1 = 5$, $m_2 = 4$ (Y)); (*b*) two flows with the same m_1 values and different m_2 values ($m_1 = 4$, $m_2 = 4$ (▲); $m_1 = 4$, $m_2 = 5$ (+)). The vertical dashed line indicates the onset of the two-travelling-wave regime ($m_2 > 0$) at $R/R_c \approx 9.6$. The data were obtained from laser-Doppler velocimetry measurements in a system with $\eta = 0.877$ whose end boundaries were both rigid.

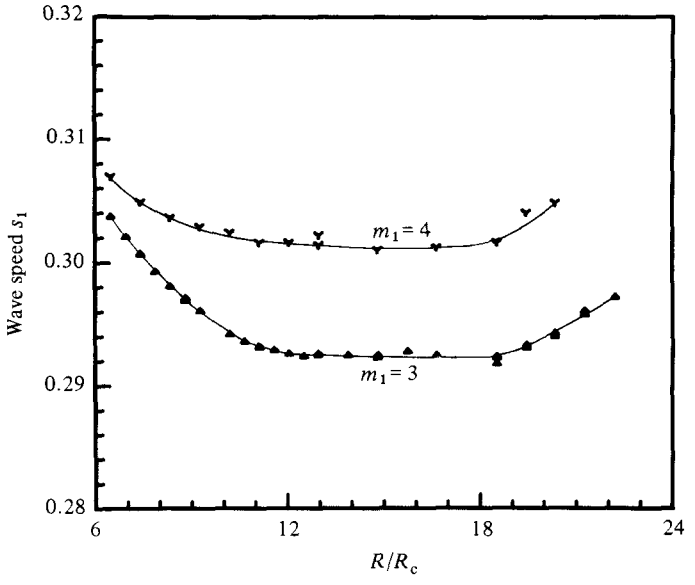

FIGURE 6. The Reynolds-number dependence of the wave speed s_1 for $m_1 = 3$ (▲) and $m_1 = 4$ (Y). Here $\bar{\lambda}/d = 2.4$, $\eta = 0.840$ and $\Gamma = 30$. The curves are drawn to guide the eye.

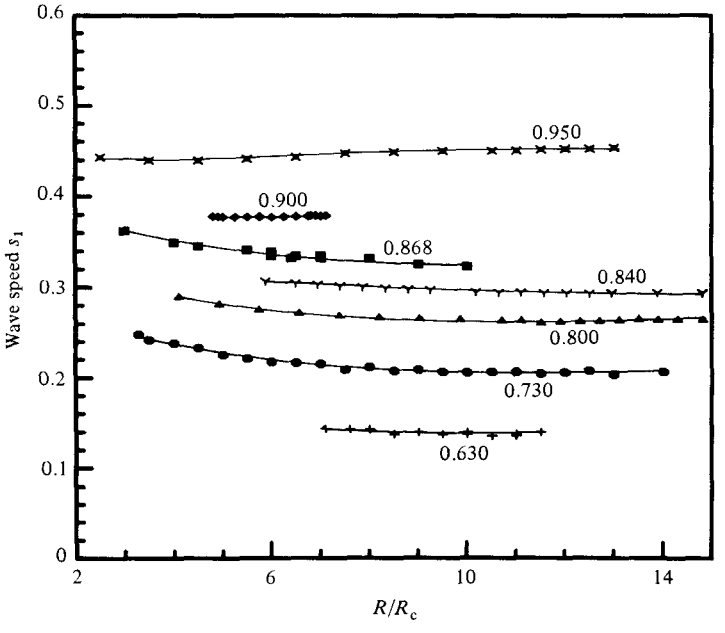

FIGURE 7. The dependence of wave speed s_1 on Reynolds number for radius ratios $\eta = 0.630$, $m_1 = 1$ (+); $\eta = 0.730$, $m_1 = 2$ (●); $\eta = 0.800$, $m_1 = 3$ (▲); $\eta = 0.840$, $m_1 = 3$ (Y); $\eta = 0.868$, $m_1 = 4$ and 5 (■); $\eta = 0.900$, $m_1 = 7$ (◆); $\eta = 0.950$, m_1 variable (×). The axial wavelength was $\bar{\lambda}/d = 2.4$ except for $\eta = 0.950$, where it was variable (see text). The curves are drawn to guide the eye.

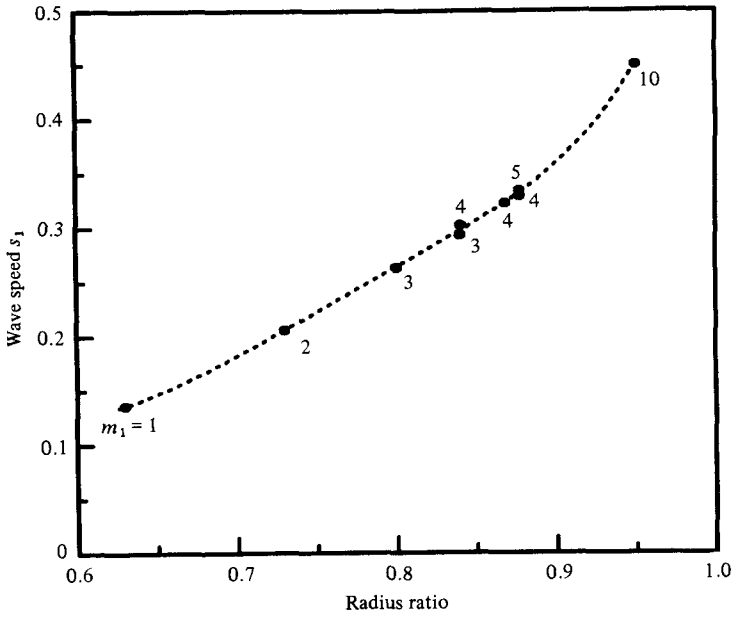

FIGURE 8. The dependence of wave speed s_1 on radius ratio at $R/R_c \approx 11.0$, which is within the region of the wave-speed plateau (see figure 7). The axial wavelength was $\bar{\lambda}/d = 2.4$ for all but two radius ratios: for $\eta = 0.877$, $\bar{\lambda}/d = 2.5$; for $\eta = 0.950$, $\bar{\lambda}$ varied owing to defects on the flow pattern. Each point is labelled with the number of azimuthal waves corresponding to that particular measurement. The curve is a best fit to the data using Chebyshev polynomials (see table 5).

where the $T_n(r)$ are the Chebyshev polynomials and c.c. denotes the complex conjugate. (The $m = -16$ and the $m = 16$ Fourier modes are indistinguishable when the velocity is evaluated at the collocation points; therefore the $m = -16$ Fourier mode is not included in the spectral sum.) Expanding the pressure field in the same way as the velocity field (4), we obtain $33 \times 32 \times 32 \times 4$ nonlinear coupled real ordinary differential equations for the spectral coefficients.

Often we exploit one or more symmetries of the flow to save computer time and storage. Some symmetries make the coefficients $\boldsymbol{a}_{n,m,k}$ identically equal to zero; other symmetries imply a relationship between the coefficients. For example, the m_1 fold shift-and-reflect symmetry of (1) requires $\boldsymbol{a}_{n,m,k} \equiv 0$ for all m not integral multiples of m_1, and

$$\hat{\boldsymbol{e}}_r \cdot \boldsymbol{a}_{n,m,k} \equiv (-1)^{m/m_1} \hat{\boldsymbol{e}}_r \cdot \boldsymbol{a}^*_{n,-m,k}, \tag{5}$$

$$\hat{\boldsymbol{e}}_\phi \cdot \boldsymbol{a}_{n,m,k} \equiv (-1)^{m/m_1} \hat{\boldsymbol{e}}_\phi \cdot \boldsymbol{a}^*_{n,-m,k}, \tag{6}$$

$$\hat{\boldsymbol{e}}_z \cdot \boldsymbol{a}_{n,m,k} \equiv -(-1)^{m/m_1} \hat{\boldsymbol{e}}_z \cdot \boldsymbol{a}^*_{n,-m,k}. \tag{7}$$

We always exploit symmetries so that the coefficients retained in the calculation are non-zero and represent (for each component of the velocity vector and for the pressure) $33 \times 32 \times 32$ *independent* pieces of information. Therefore the numerical calculation with the 6-fold-symmetric travelling wave presented in §6 includes all non-zero azimuthal Fourier modes of the form $e^{im\phi}$ with $-96 < m \leqslant 96$ and all axial modes of the form $e^{i2\pi kz/\lambda}$ with $-32 < k < 32$.

The numerical initial-value problem is solved with a fractional step method where the boundary conditions are satisfied by using a capacitance or Green-function

matrix. The details of the numerical techniques appear in Marcus (1984*a*). It can be shown that the fractional step and time-stepping errors produce a global error in the velocity $O[(\Omega^3 a^3/d^2)(\Delta t)^2, (\Omega^2 a^2/d)(\Delta t/R)]$. Unfortunately, it is impossible to predict analytically the temporal error in the wave speed s_1 because the functional dependence of s_1 on the velocity is not known; however, we have calculated the steady-state velocity and the wave speed for several values of Δt, and the errors in both the wave speed and the velocity decrease as $O[(\Omega^3 a^3/d^2)(\Delta t)^2]$. (At the Reynolds numbers of interest here ($R > 100$), the error proportional to $(\Delta t)^2$ is greater than the error proportional to $\Delta t/R$.) The smallest Δt used in the numerical calculations is $\Delta t \approx \tau/2000$, where τ is the inner-cylinder period.

We have found that the behaviour of the error in the wave speed due to finite spatial resolution is characteristic of spectral methods. In numerical calculations with very few spectral modes, the errors in the wave speed initially decrease very slowly as the number of modes is increased, but, when the resolution increases beyond a critical value, the error abruptly decreases exponentially. For example, at $R/R_c = 3$, $m_1 = 6$ and $\eta = 0.868$ we find that the error in the wave speed decreases slowly with increasing numbers of modes until there are 8 axial and 8 azimuthal modes; then the error in the wave speed decreases exponentially as more modes are added. All of the wave speeds reported in this paper were computed in the exponentially converging regime.

A complete discussion of the accuracy of the numerical code including comparisons with linear theory, internal-consistency checks and predictions of torques is given by Marcus (1984*a*) and will not be repeated here. We believe that the most sensitive test of accuracy is the comparison between the numerically predicted and the experimentally measured wave speeds. In our numerical experiments we have shown that insufficient care in treating the boundary conditions, time-splitting, or pressure evaluation can shift the computed speeds by several percent, which is easily detectable; in contrast, plots of the stream function are insensitive to subtle numerical errors. Comparisons of the numerical and laboratory values of the wave speeds are more discriminating than comparisons of the torques due to the large (several percent) experimental uncertainty in laboratory torque measurements. At the present time we cannot make a point-by-point comparison of the numerically simulated velocity field with the laboratory measurements. However, in the future we plan to mount the laser-Doppler system on a table that can rotate at the speed of the azimuthal waves; then the numerically computed velocity field can be compared directly with experiment.

Even the most accurate numerical code, one that passes all imaginable tests at some Reynolds number, will become inaccurate at sufficiently high Reynolds numbers where the range of excited wavelengths exceeds the range of numerical spatial resolution. A critical test of the spatial resolution of a spectral method is provided by plotting the kinetic energy as a function of wavenumber. Too severe a truncation in the number of modes leads to an artificial upward curl in the high-wavenumber end of the spectrum (Marcus 1981). Our spectra do not exhibit any such curl. In fact, the energy decays exponentially with increasing wavenumber, resulting in an energy in the largest wavenumber mode that is typically 10^{-14} times the energy in the smallest wavenumber mode. The energy in the highest wavenumber end of the spectrum is so small that aliasing errors are negligible. We conclude that the errors arising from the finite spatial resolution (and aliasing) are small compared with the time-stepping errors.

Some computed wave-speed values are given in table 3. These speeds were found

η	R/R_c	• λ/d	R_c	m_1	s_1	$\Delta s_1/s_1$†
0.630	7.50	2.40	73.5	1	0.146	0.01
0.868	2.00	2.14	115.1	6	0.4044	0.001
0.868	3.98	2.40	115.1	6	0.3443	0.0003
0.868	3.98	3.00	115.1	6	0.3344	0.0003
0.868	5.97	2.20	115.1	6	0.3370	0.0003
0.875	2.06	2.20	118.2	6	0.407	0.001
0.875	2.06	3.00	118.2	4	0.401	0.005
0.875	2.06	3.00	118.2	5	0.3893	0.001
0.875	2.06	3.00	118.2	6	0.3757	0.0003
0.875	2.95	3.00	118.2	6	0.352	0.005
0.875	3.89	2.32	118.2	6	0.354	0.004
0.875	3.89	3.00	118.2	6	0.342	0.004
0.875	3.89	3.90	118.2	6	0.329	0.006

† Δs_1 is the numerical uncertainty in the wave speed due to finite space and time resolution

TABLE 3. Numerically computed values of the wave speed

by extrapolating the time step to zero. The fractional uncertainty in the extrapolated wave speed due to the time-stepping error is coincidentally of the same order as the fractional difference between the wave speed computed with $\Delta t \approx \tau/2000$ and the extrapolated wave speed with $\Delta t = 0$. The uncertainties given in table 3 differ because the computations were done with different sized time steps; in the best-determined cases the uncertainty is 0.03 %.

5.2. *Analytics: a marginal stability analysis for s_1 at large R and $\eta \to 1$*

The experimental and numerical studies of flows in the Couette–Taylor system show that at large R the axially and azimuthally averaged angular momentum per unit mass $\bar{L}(r)$ is essentially independent of radius outside of the boundary layers. (In this section a horizontal bar written above a quantity will always mean the axially and azimuthally averaged component.) The value of this constant angular momentum can be computed from marginal stability theory and used to predict s_1 at large R in the limit $\eta \to 1$, as we will now show.

Figure 9 shows $\bar{L}(r) \equiv r\bar{V}_\phi$ as a function of radius. There is a boundary layer at the inner cylinder of thickness $\delta_{\text{in}} \ll d$ and a boundary layer at the outer cylinder of thickness $\delta_{\text{out}} \ll d$. Far from the boundary layers $\bar{L}(r)$ has a constant value $\bar{L}_0$. The physical explanation for $\bar{L}(r)$ being nearly constant comes from the observation that far from the boundaries the flow is well mixed. For an axisymmetric inviscid flow, Euler's equation shows that the advective derivative of the angular momentum per unit mass is zero. In a viscous flow the advective derivative of the azimuthally averaged angular momentum per unit mass is proportional to a viscous (slow) timescale, so the azimuthally averaged angular momentum per unit mass in a Lagrangian frame is nearly constant, i.e. an adiabatic invariant. Since the fluid is well mixed, the adiabatic invariant is well mixed, and hence the angular momentum per unit mass is constant far from the boundary layers.

Marcus (1984*b*) has found that the one-travelling-wave flows have a comoving surface such that all fluid on this surface has the same azimuthal angular velocity as the travelling-wave speed s_1. The radius of the comoving surface, although a function of ϕ, z and t, never extends into the boundary layers. In numerical simulations the azimuthal velocity is always dominated by V_ϕ; therefore we expect

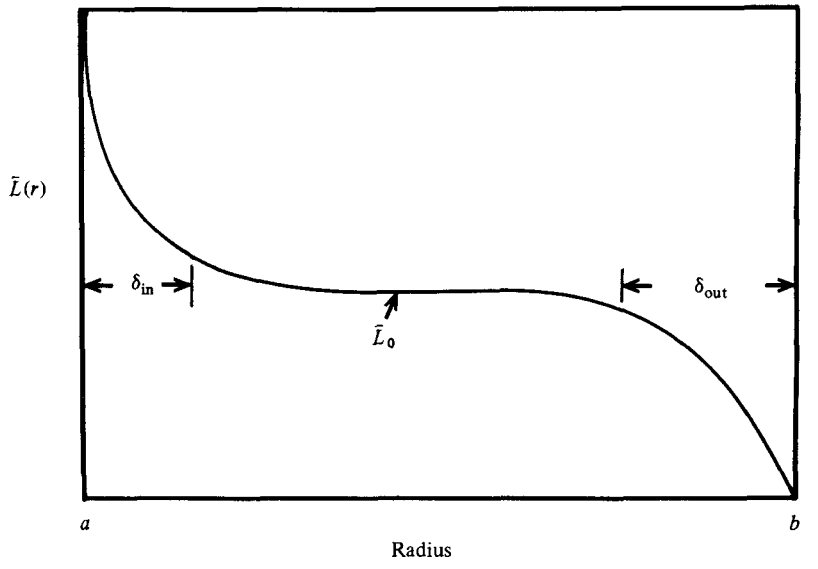

FIGURE 9. The radial dependence of the axially and azimuthally averaged angular momentum per unit mass $\bar{L}(r)$, shown schematically at large R where $\bar{L}(r)$ is essentially constant outside of the narrow boundary layers of thickness δ_{in} and δ_{out} at the inner and outer cylinders respectively.

that the angular velocity of the comoving surface (and hence the speed of the travelling wave) will be about $\bar{L}(r_c)/r_c^2$, where r_c is the average radius of the comoving surface. Assuming that $\bar{L}_0$ is constant and that $r_c \approx \frac{1}{2}(a+b)$, a numerical error of Δr_c in the calculation of r_c produces a fractional error in the angular velocity of the wave of

$$\frac{\Delta s_1}{s_1} \approx \frac{4(1-\eta)}{1+\eta}\left(\frac{\Delta r_c}{d}\right). \tag{8}$$

For large radius ratio, the fractional error $\Delta s_1/s_1$ approaches zero. In the limit $\eta \to 1$ the angular velocity of the comoving surface (or s_1) is $\bar{L}_0/a^2$.

The values of $\bar{L}_0$, δ_{in}, δ_{out}, and the torque per unit axial length G are calculated in the Appendix using marginal stability theory. That analysis yields

$$\frac{\delta_{in}}{d} = 1.14\left(\frac{R}{R_c}\right)^{-\frac{2}{3}}, \tag{9}$$

$$\frac{\delta_{out}}{d} = 1.47\left(\frac{R}{R_c}\right)^{-\frac{2}{3}}, \tag{10}$$

$$\frac{G}{G_{cc}} = 0.383\left(\frac{R}{R_c}\right)^{\frac{2}{3}}, \tag{11}$$

$$\frac{\bar{L}_0}{\Omega a^2} = 0.563. \tag{12}$$

Here G_{cc} is the torque per unit axial length for circular Couette flow (for $\eta \approx 1$):

$$\frac{G_{cc}}{\rho\Omega^2 a^4} = 0.1517\left(\frac{R}{R_c}\right)^{-1}(1-\eta)^{\frac{1}{2}}, \tag{13}$$

where R_c in the limit $\eta \to 1$ is given by (Chandrasekhar 1961, p. 303)

$$R_c \approx 41.41(1-\eta)^{-\frac{1}{2}}. \tag{14}$$

Equations (9)–(12) are only valid for $\eta \to 1$ and $R \gg R_c$, $\delta_{in} + \delta_{out} \ll d$ and $G/G_{cc} > 1$. Observe that the inner and outer boundary layers do not have the same thickness. Also note that δ_{in} and δ_{out} depend on R, but $\bar{L}_0/\Omega a^2$ is *independent* of Reynolds number.

In the limit $\eta \to 1$ the angular velocity of the comoving surface is the wave speed. Thus the marginal stability analysis leads to the prediction for R sufficiently large:

$$s_1 = \frac{\bar{V}_\phi}{a} = 0.563\Omega \quad (\eta \approx 1). \tag{15}$$

If R is large enough for marginal stability theory to be valid, then s_1 is independent of R, m_1 and λ. The same kind of analysis should apply to the second travelling wave, so (15) should describe s_2 as well as s_1.

6. Comparison of experiments with the numerical and analytic studies

The numerical simulations are most accurate and least costly for low values of R; as R is increased, more Fourier and Chebyshev modes are needed to fully resolve the flow velocity. On the other hand, the laboratory measurements extrapolated to infinite aspect ratio are most accurate and least time-consuming at high values of R; at low values of R the extrapolation to infinite aspect ratio (which is the aspect ratio in the numerical computations) has the most uncertainty. Furthermore, as the Reynolds number is decreased, the time it takes for the fluid to relax to equilibrium increases; thus at small R it becomes prohibitively time-consuming to complete a series of measurements determining the infinite-aspect-ratio limit of s_1. Therefore, as a compromise between numerical and laboratory convenience, we have chosen to compare wave speeds at two intermediate Reynolds numbers.

The functional form of the aspect-ratio dependence of the wave speed is not known from theory. We have examined several possible forms of $s_1(\Gamma)$, including those given by (2) and (3). There are systematic departures of the data from both (2) and (3), but the departures are in opposite directions, leading to estimates for $s_1(\Gamma = \infty)$ that are probably too low (s_1^α, equation (2)) and too high (s_1^β, equation (3)) (see figure 2). However, $s_1^\alpha(\infty)$ and $s_1^\beta(\infty)$ typically differ by 0.3 % for the cases we have examined. Thus the best estimate we can make for the experimentally determined value of $s_1(\infty)$ is the average of $s_1^\alpha(\infty)$ and $s_1^\beta(\infty)$; the uncertainty in this average is 0.2 %.

The computed and measured wave speeds for the cases that can be directly compared differ by less than 0.1 %, which is well within the experimental uncertainty (see table 4).

The three cases for which the measured and computed wave speeds can be directly compared all have $s_1 \approx 0.33$. The wave speed has also been computed for a case with a much smaller wave speed: $s_1 = 0.146 \pm 0.001$ at $\eta = 0.630$, $R/R_c = 7.5$, $\lambda/d = 2.4$ and $m_1 = 1$. Our measurements at this η cannot be directly compared with the computed wave speed because the aspect ratio dependence has not been measured (and cannot be measured with the existing apparatus); however, the wave speed measured at a small aspect ratio ($s_1 = 0.149$ at $\Gamma \approx 26$) is in good qualitative agreement with that computed for an infinite cylinder.

In order to compare the measurements with the prediction of the marginal stability analysis, we have extrapolated the data to $\eta = 1$, as shown in figure 10 (see also table

		s_1	
R/R_c	$\bar{\lambda}/d$	computed	measured†
3.98	2.4	0.3443 ± 0.0001	0.3440 ± 0.0008
3.98	3.0	0.3344 ± 0.0001	0.3347 ± 0.0007
5.97	2.2	0.3370 ± 0.0001	0.3370 ± 0.0002

† The average of $s_1^{\alpha}(\infty)$ and $s_1^{\beta}(\infty)$ from table 2

TABLE 4. Comparison of computed and measured wave speeds ($\eta = 0.868$, $m_1 = 6$)

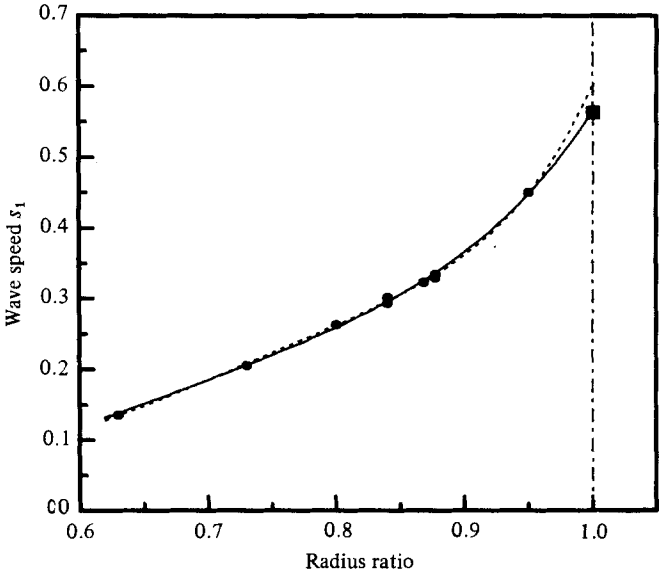

FIGURE 10. A comparison of the marginal stability prediction (■) at $\eta = 1$ with an extrapolation of the data of figure 8. The data (●) have been fitted with Chebyshev polynomials (– –) and a quartic polynomial (——).

5). A fit of the data (including the wave-speed value at $\eta = 0.507$ reported by Brandstäter, Pfister & Schulz-DuBois 1982) to a quartic polynomial yields $s_1(\eta = 1) = 0.563$, in excellent agreement with the predicted value $s_1 = 0.563$! The agreement is not so good when the data are fitted to Chebyshev polynomials, yielding $s_1(\eta = 1) = 0.602$; however, Chebyshev polynomials are known to be poor functions for extrapolation because of the heavy weight given to the endpoints.

7. Comparison with other work

7.1. *Comparison with other experiments*

There have been very few previous studies of the dependence of the wave speed on the control parameters or on the spatial state ($\bar{\lambda}, m_1, m_2$), even though the wave speed is a rather simple quantity to measure.

As mentioned previously, Coles found that $s_1 \to \frac{1}{3}$ at large R, independently of m_1 and $\bar{\lambda}$ (Γ and η were fixed). We find that in general there is some range in R over

Function	Parameters					r.m.s. deviation %	$s_1(\eta = 1)$
	a	b	c	d	e		
† Quartic polynomial	3.391	−20.339	45.232	−43.510	15.789	0.35	0.563
‡ Chebyshev polynomial	0.369	0.436	−0.332	0.106	0.023	0.26	0.602

† $s_1(\eta) = a + b\eta + c\eta^2 + d\eta^3 + e\eta^4$

‡ $s_1(\eta) = a + bT_4(\eta) + cT_5(\eta) + dT_6(\eta) + eT_8(\eta)$

TABLE 5. Quartic and Chebyshev fits of s_1 versus η

which s_1 is essentially constant, as figure 7 illustrates, but at large R there is a small increase in s_1 before the waves disappear. The Reynolds number at which s_1 begins to increase depends on η, m_1 and $\bar{\lambda}$ as well as R.

No previous study to our knowledge has examined the dependence of s_1 on aspect ratio, even though the aspect ratio is known to have a profound influence on the flow states (Cole 1976; Benjamin 1978; Donnelly *et al.* 1980; King & Swinney 1983).

The dependence of s_1 on $\bar{\lambda}$ has been investigated in two studies done for $R/R_c < 2$ (Snyder 1969; Ahlers *et al.* 1983); s_1 was found to decrease with increasing $\bar{\lambda}$. Our experiments show that s_1 can also increase with increasing $\bar{\lambda}$, or, as figure 4 illustrates, can even exhibit an extremum.

Ahlers *et al.* also found that the wave speed was a function of m_1. They observed that when m_1 was increased from three to four, and, at a different $\bar{\lambda}$, from four to five, s_1 decreased. We have also observed s_1 to decrease with increasing m_1, but not universally; figures 5(*a*) and 6 show two instances where the opposite relationship occurs.

The only previous measurements of the wave speed as a function of η were those of Cole (1981, 1983) at the *onset* of wavy vortex flow. He found that for $\eta < 0.75$ the wave speed at onset was much less than the often-quoted value of $\frac{1}{2}\Omega$; similarly, our figures 7 and 8 show that the wave speed at large R can be quite different from the often quoted value of $\frac{1}{3}\Omega$.

The wave speed has been measured by Brandstäter *et al.* (1982) at $\eta = 0.507$, a radius ratio smaller than our smallest value, $\eta = 0.630$; their result $s_1 = 0.08$ is consistent with an extrapolation of our data in figure 8.

7.2. *Comparison with other numerical work*

Analytically, it is impossible to calculate the wave speed with no approximations. Numerically, it is easiest to compute the speed of the one-travelling-wave flow at Reynolds number $R_{\text{onset}}(\lambda, m_1)$, which is the Reynolds number at which a Taylor-vortex flow with axial wavelength λ becomes unstable to a one-travelling-wave flow with azimuthal wavenumber m_1 and axial wavelength λ. At R_{onset} the non-axisymmetric component of the velocity has infinitesimal amplitude. The wave speed is determined by two numerical calculations: first, the *nonlinear*, steady-state, axisymmetric Taylor-vortex flow is determined; secondly, the eigenvalues of the non-axisymmetric *linear* perturbations of the Taylor-vortex flow are computed. The imaginary part of the eigenvalue is the growth rate of the linear perturbation (and is zero by definition at R_{onset}) and the real part of the eigenvalue is the wave speed. Jones (1981) has used this procedure with 14 radial Chebyshev and 7 axial Fourier modes to compute the nonlinear Taylor vortex flow to find wave speeds for flows with

$\lambda/d = 2.01$, $\eta = 0.8756$, $m < 12$ and $R/R_c \leqslant 4.0$. At $R/R_c = 4.0$ the speeds calculated by Jones and our measured speeds differ by about 5 % (after the appropriate radius ratio corrections have been made), but Jones' numerical method is not, of course, applicable for $R > R_{onset}(\lambda, m_1)$, where the travelling wave has finite amplitude. Unfortunately, in most cases it is not possible to make a direct comparison between numerical computations at $R_{onset}(\lambda, m_1)$ and laboratory measurements, because at $R = R_{onset}$ most one-travelling-wave flows are unstable to $m \neq m_1$ perturbations and cannot be observed experimentally. For example, the $m_1 = 6$ one-travelling-wave flow has finite amplitude and is stable for $R/R_c \geqslant 2.1$ for $\eta = 0.868$ and $\lambda/d = 3$, but when the Reynolds number is decreased to $R = R_{stab}(\lambda, m_1) > R_{onset}(\lambda, m_1)$ the travelling wave still has finite amplitude but becomes unstable to an $m_1 = 4$ one-travelling-wave flow (Marcus 1984*b*); hence the $m_1 = 6$ one-travelling-wave flow cannot be experimentally observed with $R < R_{stab}(\lambda, m_1)$.

The small (5 %) difference between the wave speeds computed by Jones and the experimental values shows that the wave speed is not very sensitive to the finite amplitude of the travelling wave. This lack of sensitivity is explained in part by the functional form of the azimuthal wave speed, $\bar{V}_\phi \approx \bar{L}(r)/r$, shown for large R in figure 9 and discussed in §5.2. Since $\bar{L}(r)$ is not a strong function of radius and since the radius of the comoving surface $r_c \approx \frac{1}{2}(b+a)$, (8) shows that a numerical error in the calculation of the comoving surface of Δr_c produces a fractional error of only about $0.265\Delta r_c/d$ in the wave speed. A 5 % error in s_1 requires $\Delta r_c/d \leqslant \frac{1}{5}$.

8. Conclusions

8.1. *Experimental results*

We have conducted the first exploratory study of the dependence of wave speed on the geometry and forcing and on the intrinsic axial and azimuthal wavelengths. Our experiments show that the dependence of s_1 on R, Γ, η, $\bar{\lambda}$, m_1 and m_2 is in general very complex. However, at large R, s_1 depends primarily only on η, increasing monotonically threefold in the range studied ($0.63 \leqslant \eta \leqslant 0.95$), as shown in figure 8. In contrast, the variation of s_1 with Γ, R, $\bar{\lambda}$, m_1 and m_2 is, for a given η, only of the order of a few percent, as figures 2–7 illustrate. No generalization can be made about the weak dependence of s_1 on $\bar{\lambda}$, m_1, m_2 and Γ – in some cases s_1 decreases with increasing values of these parameters, while in other cases s_1 increases.

Since s_1 depends on so many variables, it has of course not been possible to survey completely the dependence of s_1 on every variable. The dependence of s_1 on R was examined at each η for $\bar{\lambda}$ equal to or near $2.4d$, and two or more values of m_1 were examined at each η except $\eta = 0.630$, where only the $m_1 = 1$ state was observed. However, the dependence of s_1 and s_2 on Γ was investigated only for $\eta = 0.868$, and the dependence of s_1 on m_2 only for $\eta = 0.877$. Future experiments can extend the study of s_1 beyond the parameter ranges examined here and can examine the behaviour of the wave speeds of other azimuthal travelling-wave modes.

8.2. *Numerics*

We have developed a simulation of the Couette–Taylor system that is valid at Reynolds numbers well beyond the onset of Taylor vortex flow. Extensive self-consistency tests have been applied to this code. Wave speeds determined in the simulations have been compared with measured wave speeds at $\eta = 0.868$ for several different values of R, m_1 and λ. The calculated and measured wave speeds agree to

within 0.1 % in the best-determined cases. We know of no other simulation of any flow that achieves such accuracy at comparable Reynolds numbers.

Now that the validity of the simulation has been demonstrated in the present work, it will be possible in the future to use the numerical code to gain insight into the physical mechanisms of different instabilities in the Couette–Taylor system. The simulations are too expensive to permit wide-ranging exploratory studies of the dependence of the flow on different parameters such as have been obtained in our measurements of the wave speeds. On the other hand, the simulations yield information on the entire velocity field at each instant of time, information not readily obtainable from experiments. Simulations using our code should be particularly helpful in understanding the essential differences in the variety of flows that have been observed with both cylinders rotating independently at different speeds (Andereck, Dickman & Swinney 1983; Andereck, Liu & Swinney 1984).

Comparisons of the measured and calculated wave speeds and studies of energy spectra (Marcus 1984*a*) indicate that our code with 33 radial Chebyshev modes, 32 Fourier azimuthal modes, and 32 Fourier axial modes has a sufficient number of modes to prevent severe modal-truncation artifacts even at Reynolds numbers as large as $R \approx 1400$. However, at this large Reynolds number some numerically created pile-up of the energy becomes noticeable in the high-wavenumber end of the spectrum. Thus the previously reported codes with much smaller numbers of modes would produce serious errors in the wave speeds at these Reynolds numbers. The question of how many modes are necessary to represent the flow accurately at different Reynolds numbers is an important one that should be addressed in a future study.

In the past the contact between numerical and experimental studies has usually been made by comparing calculated and measured torques. We consider the wave speed to be a better test of numerical predictions since wave speeds can be measured with an accuracy of better than 0.1 % for a given set of values of the experimental parameters, which is considerably better than the usual torque measurements. In either case, contact with theory must be made by extrapolating the measurements to infinite aspect ratio. For wave speeds this can be done straightforwardly though tediously, with an accuracy of 0.2 % or better, as we have shown.

8.3. *Analytics*

We have presented an approximate stability analysis, based on plausible but unproven assumptions, which predicts that the wave speed at large Reynolds number in the small gap limit ($\eta = 1$) should approach the value 0.563Ω. This prediction should apply equally well to all travelling azimuthal wave modes. The agreement between the prediction and the extrapolation of our measured wave speeds for the first travelling wave is remarkably good.

We thank Leslie Reith for making the laser-Doppler velocimetry measurements; David Andereck, Anke Brandstäter and Li-Hua Zhang for helpful discussions; and Mike Biggerstaff, Philip Dixon, Michael S. Brown, Ignazio Ciufolini, Steve Stotts and Bright Dornblaser for help in the experiments. The experiments were conducted at the University of Texas with the support of National Science Foundation Grant MEA82-06889, and the theoretical work was conducted at MIT with the support of National Science Foundation Grant MEA82-15695. The numerical simulations were carried out on the CRAY-1 computer of the National Center for Atmospheric Research, which is sponsored by the National Science Foundation.

Appendix. Marginal stability theory (for $R \gg R_c$ and $\eta \approx 1$)

Using marginal stability arguments in a manner analogous to their use in convection (Robinson 1967), we now derive relationships for the boundary-layer thicknesses δ_{in} and δ_{out} (see figure 9), the axially and azimuthally averaged angular momentum per unit mass $\bar{L}(r)$ and the torque per unit axial length G. The analysis is valid only in the limit $\eta \to 1$ and $R \gg R_c$.

Our principal assumption is that the thicknesses of the inner and outer boundary layers are determined by centrifugal instability. More specifically, it is assumed that the inner and outer boundary layers form marginally stable circular Couette flows. The *gedanken* Couette system formed by the inner boundary layer is confined between the real cylinder at radius a and an imaginary outer cylinder at $a+\delta_{in}$; the inner cylinder has an angular velocity of Ω and the imaginary outer cylinder an angular velocity equal to that of the fluid at $a+\delta_{in}$. Similarly, the *gedanken* Couette system formed by the outer boundary layer is confined between an imaginary outer cylinder at radius $b-\delta_{out}$ and the real cylinder at radius b; the imaginary inner cylinder has an angular velocity equal to that of the fluid at $b-\delta_{out}$ and the outer cylinder an angular velocity of zero. Now a circular Couette flow between rigid cylinders with inner and outer radii r_1 and r_2 and inner and outer cylinder angular velocities Ω_1 and Ω_2 is marginally stable when (Chandrasekhar 1961, p. 303)

$$\frac{\Omega_1^2 r_1 (r_2-r_1)^3}{\nu^2}\left(1-\frac{\Omega_2}{\Omega_1}\right)\left(1+\frac{\Omega_2}{\Omega_1}\right) \approx T_c, \tag{A 1}$$

where ν is the kinematic viscosity of the fluid, and T_c, the critical Taylor number, has the value 1715 for $0 < \Omega_2 < \Omega_1$ and $\eta \approx 1$. Although the appropriate values of T_c would differ from 1715 since the no-slip boundary condition is not satisfied for the boundary-layer systems at the imaginary-cylinder walls formed by the fluid, this does not materially affect our argument. The fluid in a boundary layer, of course, does not have the velocity profile of circular Couette flow. Smith & Townsend (1982) have experimentally measured the velocity in the boundary layer and found that for very large R the velocity falls off approximately as $\log r$, as in a wall-bounded shear flow. The exact velocity profile of the boundary layer is not of importance in this calculation, but we shall assume that the *thickness* of the boundary layer is determined by centrifugal instability and not by shear forces. Treating the flow in the inner boundary layer as if it were a marginally stable circular Couette flow, we have $r_1 = a$, $\Omega_1 = \Omega$, $r_2 = a+\delta_{in}$ and $\Omega_2 = \bar{L}_0/(a+\delta_{in})^2$ in (A 1); hence

$$\left(\frac{\Omega^2 \delta_{in}^3 a}{\nu^2}\right)\left(1-\frac{\bar{L}_0}{\Omega(a+\delta_{in})^2}\right)\left(1+\frac{\bar{L}_0}{\Omega(a+\delta_{in})^2}\right) = T_c. \tag{A 2}$$

Similarly, for the outer boundary layer we have $r_1 = b-\delta_{out}$, $\Omega_1 = \bar{L}_0/(b-\delta_{out})^2$, $r_2 = b$ and $\Omega_2 = 0$; hence

$$\frac{\bar{L}_0^2 \delta_{out}^3}{(b-\delta_{out})^3 \nu^2} = T_c. \tag{A 3}$$

In an equilibrium flow, the torque that the inner cylinder exerts on the fluid is equal to the torque that the fluid exerts on the outer cylinder. The torque (per unit axial length) at the outer cylinder is

$$G_{out} = -2\pi\rho\nu b^2 \left(\frac{\partial V_\phi}{\partial r}-\frac{V_\phi}{r}\right)\Bigg|_{r=b}, \tag{A 4}$$

where ρ is the fluid density. The term V_ϕ/r in (A 4) is negligible compared with $\partial V_\phi/\partial r$ in the limit $\eta \to 1$. Therefore we have

$$G_{\text{out}} \approx 2\pi\rho\nu b \frac{\bar{L}_0}{\delta_{\text{out}}}. \tag{A 5}$$

Similarly, the torque exerted at the inner cylinder is

$$G_{\text{in}} = -2\pi\rho\nu a^2 \left(\frac{\partial V_\phi}{\partial r} - \frac{V_\phi}{r}\right)\Big|_{r=a}$$

$$\approx 2\pi\rho\nu a^2 \left(\frac{a\Omega - \bar{L}_0/a}{\delta_{\text{in}}}\right). \tag{A 6}$$

Setting $G = G_{\text{in}} = G_{\text{out}}$, using (A 2), (A 3), (A 5) and (A 6), and taking the limit $\eta \to 1$, we obtain

$$\frac{\delta_{\text{in}}}{d} = 1.14 \left(\frac{R}{R_c}\right)^{-\frac{2}{3}}, \tag{A 7}$$

$$\frac{\delta_{\text{out}}}{d} = 1.47 \left(\frac{R}{R_c}\right)^{-\frac{2}{3}}, \tag{A 8}$$

$$\frac{G}{G_{\text{cc}}} = 0.383 \left(\frac{R}{R_c}\right)^{\frac{2}{3}}, \tag{A 9}$$

$$\frac{\bar{L}_0}{\Omega a^2} = \frac{1}{1 + \delta_{\text{in}}/\delta_{\text{out}}} = 0.563. \tag{A 10}$$

We have expressed the torque in (A 9) in units of G_{cc}, the analytic value of the torque per unit axial length in circular Couette flow (see (13) in §5.2). The quantity G/G_{cc} is the analogue of the Nusselt number in thermal convection. The analysis leading to (A 7)–(A 10) applies only when the boundary layers are well defined, that is, when $R \gg R_c$; in this limit (A 7) and (A 8) yield $\delta_{\text{in}} + \delta_{\text{out}} \ll d$.

Our expressions for δ_{in}, δ_{out} and G/G_{cc} differ from those obtained by Batchelor (1960), whose derivation assumed that the boundary layers at the inner and outer cylinders were connected by boundary layers between the Taylor vortices. Batchelor's estimates for the boundary-layer thicknesses (which he assumed to be equal) and G/G_{cc} are proportional to $(R/R_c)^{-\frac{1}{2}}$ and $(R/R_c)^{\frac{1}{2}}$ respectively. Unfortunately, there are insufficient experimental data at high R and $\eta \approx 1$ to distinguish between Batchelor's formulae and ours.

Barcilon *et al.* (1979) derive relationships for the torque and boundary-layer thicknesses that have the same dependence on R/R_c (although not the same dependence on η) as ours. Barcilon *et al.* assume that the boundary layer is filled with Görtler vortices. The boundary-layer thickness is then defined to be equal to the diameter of the Görtler vortices. Since the Görtler instability and the circular Couette instability are both centrifugally driven, it is not surprising that the diameter of the Görtler vortices is the same as the thickness of a marginally stable (with respect to centrifugal instability) boundary layer. However, to use marginal stability theory, it is not necessary that the boundary layer be actually filled with Görtler vortices. For example, when marginal stability analysis is used to compute boundary-layer thicknesses and the Nusselt number in thermal convection, the boundary layer is viewed as a shear layer in which an infinitesimal thermal perturbation can cause convective instability. The boundary layer is not filled with small convection cells.

Similarly, we view the boundary layer in Tayalor–Couette flow as a shear layer in which an infinitesimal perturbation can cause a centrifugal instability.

Finally, both Batchelor's assumption that the thicknesses of the boundary layers at the outer and inner cylinders are equal and the assumption of Barcilon *et al.* that the mean azimuthal velocity is $\overline{V}_\phi = \frac{1}{2}\Omega a$ lead to the prediction that the wave speed in wavy-vortex flow would have an angular velocity of $\frac{1}{2}\Omega$ in the limit $\eta \to 1$, while (A 10) predicts a wave speed of 0.563Ω.

REFERENCES

Abernathy, F. H., Bertschy, J. R., Chin, R. W. & Keyes, D. E. 1980 Polymer induced fluctuations in high strain-rate laminar flows. *J. Rheol.* **24**, 647.

Ahlers, G., Cannell, D. S. & Dominguez Lerma, M. A. 1983 Possible mechanism for transitions in wavy Taylor-vortex flow. *Phys. Rev.* **A27**, 1225.

Andereck, C. D., Dickman, R. & Swinney, H. L. 1983 New flows in a circular Couette system with co-rotating cylinders. *Phys. Fluids* **26**, 1395.

Andereck, C. D., Liu, S. S. & Swinney, H. L. 1984 Flow regimes in a circular Couette system with independently rotating cylinders. Submitted to *J. Fluid Mech.*

Barcilon, A., Brindley, J., Lessen, M. & Mobbs, F. R. 1979 Marginal instability in Taylor–Couette flows at a very high Taylor number. *J. Fluid Mech.* **94**, 453.

Batchelor, G. K. 1960 Appendix to Donnelly, R. J. & Simon, N. J. 'An empirical torque relation for supercritical flow between rotating cylinders'. *J. Fluid Mech.* **7**, 401.

Benjamin, T. B. 1978 Bifurcation phenomena in steady flows of a viscous fluid. II. Experiments. *Proc. R. Soc. Lond.* A **359**, 27.

Berman, N. S. 1978 Drag reduction by polymers. *Ann. Rev. Fluid Mech.* **10**, 47.

Brandstäter, A., Pfister, G. & Schulz-DuBois, E. O. 1982 Excitation of a Taylor vortex mode having resonant frequency dependence of coherence length. *Phys. Lett.* **88A**, 407.

Burkhalter, J. E. & Koschmieder, E. L. 1973 Steady supercritical Taylor vortex flow. *J. Fluid Mech.* **58**, 547.

Chandrasekhar, S. 1961 *Hydrodynamic and Hydromagnetic Stability.* Oxford University Press.

Cole, J. A. 1976 Taylor-vortex instability and annulus-length effects. *J. Fluid Mech.* **75**, 1.

Cole, J. A. 1981 Wavy vortex onset and cylinder radius ratio. Taylor Vortex Flow Working Party. Second meeting, Tufts University, Medford, Mass., June 1981 (unpublished).

Cole, J. A. 1983 The effect of cylinder radius ratio on wavy vortex onset. Taylor Vortex Flow Working Party, Third meeting, Nancy, France, 1983 (unpublished).

Coles, D. 1965 Transition in circular Couette flow. *J. Fluid Mech.* **21**, 385.

Davey, A., Di Prima, R. C. & Stuart, J. T. 1968 On the instability of Taylor vortices. *J. Fluid Mech.* **31**, 17.

Di Prima, R. C. & Swinney, H. L. 1981 Instabilities and transition in flow between concentric rotating cylinders. In *Hydrodynamic Instabilities and the Transition to Turbulence* (ed. H. L. Swinney & J. P. Gollub), p. 139. Springer.

Donnelly, R. J., Park, K., Shaw, R. & Walden, R. W. 1980 Early nonperiodic transitions in Couette flow. *Phys. Rev. Lett.* **44**, 987.

Fenstermacher, P. R., Swinney, H. L. & Gollub, J. P. 1979 Dynamical instabilities and the transition to chaotic Taylor vortex flow. *J. Fluid Mech.* **94**, 103.

Feynman, R. P., Leighton, R. B. & Sands, M. 1964 *The Feynman Lectures on Physics*, vol. II, p. 41-11. Addison-Wesley.

Gorman, M., Reith, L. A. & Swinney, H. L. 1980 Modulation patterns, multiple frequencies, and other phenomena in circular Couette flow. *Ann. NY Acad. Sci.* **357**, 10.

Gorman, M. & Swinney, H. L. 1982 Spatial and temporal characteristics of modulated waves in the circular Couette system. *J. Fluid Mech.* **117**, 123.

Gorman, M., Swinney, H. L. & Rand, D. A. 1981 Doubly periodic circular Couette flow: experiments compared with predictions from dynamics and symmetry. *Phys. Rev. Lett.* **46**, 992.

JEFFERY, G. B. 1923 The motion of ellipsoidal particles immersed in a viscous fluid. *Proc. R. Soc. Lond.* A **102**, 161.

JONES, C. A. 1981 Nonlinear Taylor vortices and their stability. *J. Fluid Mech.* **102**, 249.

KING, G. P. & SWINNEY, H. L. 1983 Limits of stability and irregular flow patterns in wavy vortex flow. *Phys. Rev.* **A27**, 1240.

LORENZEN, A., PFISTER, G. & MULLIN, T. 1983 End effects on the transition to time-dependent motion in the Taylor experiment. *Phys. Fluids* **26**, 1.

L'VOV, V. S., PREDTECHENSKY, A. A. & CHERNYKH, A. I. 1981 Bifurcation and chaos in a system of Taylor vortices: a natural and numerical experiment. *Sov. Phys. JETP* **53**, 562.

MARCUS, P. S. 1981 Effects of truncation in modal representations of thermal convection. *J. Fluid Mech.* **103**, 241.

MARCUS, P. S. 1984*a* Simulation of Taylor–Couette flow – numerical methods and comparison with experiment. Submitted to *J. Fluid Mech.*

MARCUS, P. S. 1984*b* Simulation of Taylor–Couette flow – numerical results for wavy vortex flow with one travelling wave. Submitted to *J. Fluid Mech.*

MULLIN, T. & BENJAMIN, T. B. 1980 Transition to oscillatory motion in the Taylor experiment. *Nature* **288**, 567.

PARK, K., CRAWFORD, G. L. & DONNELLY, R. J. 1983 Characteristic lengths in the wavy vortex state of Taylor–Couette flow. *Phys. Rev. Lett.* **51**, 1352.

ROBINSON, J. L. 1967 Finite amplitude convection cells. *J. Fluid Mech.* **30**, 577.

SHAW, R. S., ANDERECK, C. D., REITH, L. A. & SWINNEY, H. L. 1982 Superposition of travelling waves in the circular Couette system. *Phys. Rev. Lett.* **48**, 1172.

SMITH, G. P. & TOWNSEND, A. A. 1982 Turbulent Couette flow between concentric cylinders at large Taylor numbers. *J. Fluid Mech.* **123**, 187.

SNYDER, H. A. 1969 Change in wave-form and mean flow associated with wavelength variations in rotating Couette flow. Part 1. *J. Fluid Mech.* **35**, 337.

SNYDER, H. A. 1970 Waveforms in rotating Couette flow. *Intl J. Non-Linear Mech.* **5**, 659.

ZAKIN, J. L., NI, C. C., HANSEN, R. J. & REISCHMAN, M. N. 1977 Laser Doppler velocimetry studies of early turbulence. *Phys. Fluids Suppl.* **20**, S85.

ZHANG, L. H. & SWINNEY, H. L. 1984 Wavy modes in turbulent Taylor vortex flow. Submitted to *J. Fluid Mech.*